Optics Letters

Mode-locked fiber laser based on chalcogenide microwires

Alaa Al-Kadry,[1,*] Mohammed El Amraoui,[2] Younès Messaddeq,[2] and Martin Rochette[1]

[1]Department of Electrical and Computer Engineering 3480 University Street, McGill University, Montréal (Québec) H3A 0E9, Canada
[2]COPL, 2375 rue de la Terrasse, Laval University Québec (Québec), G1 V 0A6, Canada
*Corresponding author: alaa.al-kadry@mail.mcgill.ca

Received 2 July 2015; revised 10 August 2015; accepted 12 August 2015; posted 17 August 2015 (Doc. ID 244139); published 11 September 2015

We report the first mode-locked fiber laser using a chalcogenide microwire as the nonlinear medium. The laser is passively mode-locked with nonlinear polarization rotation and can be adjusted for the emission of solitons or noise-like pulses. The use of the microwire leads to a mode-locking threshold at the microwatt level and shortens the cavity length by 4 orders of magnitude with respect to other lasers of its kind. The controlled birefringence of the microwire, combined with a linear polarizer in the cavity, enables multiwavelength laser operation with tunable central wavelength, switchable wavelength separation, and a variable number of laser wavelengths.

OCIS codes: (140.0140) Lasers and laser optics; (230.0230) Optical devices; (140.3510) Lasers, fiber; (190.4370) Nonlinear optics, fibers.

http://dx.doi.org/10.1364/OL.40.004309

Passively mode-locked and multiwavelength lasers are attractive due to their multiple applications in wavelength division multiplexed systems, optical sensors, and spectroscopy [1–3]. Several techniques have been proposed for fiber lasers to operate on a soliton [4–7] and noise-like [8] pulse generation regime, as well as a multiwavelength emission regime [9–12]. These regimes of laser operation are in demand for diverse technologies [1]. It is thus convenient for practical applications to enable one fiber laser to operate on a pulse generation regime as well as on a multiwavelength emission regime. Fiber lasers that were reported with multiple operation regimes required a hundred [13] to a thousand [14,15] meters of optical fiber to incur sufficient nonlinear optical interaction within the laser cavity. Practically, there is a continued effort from researchers to achieve a stable and reliable fiber laser while offering low power consumption, compactness, and controllable path-averaged cavity dispersion.

Chalcogenide (ChG) fibers are excellent candidates to reduce the cavity length of fiber lasers since their nonlinearity is up to ~930 times that of a single-mode fiber (SMF) made of silica [16,17]. The nonlinearity can be increased further by tapering down the diameter of a ChG fiber to the micrometer range to form a microwire [18,19]. We have recently fabricated ChG As_2Se_3 microwires surrounded by a protective polymethyl methacrylate (PMMA) coating and observed a high waveguide nonlinearity of $\gamma = 185\ W^{-1}\,m^{-1}$ [20]. The PMMA coating provides mechanical strength for the normal handling of the microwire, while preventing evanescent light interaction with the surrounding environment. The extreme nonlinearity of ChG microwires allows for fiber laser operation at low threshold powers. In addition, the waveguide dispersion of microwires can be engineered to balance the path-averaged cavity dispersion [21]. The net dispersion of the laser cavity plays a critical role for generating a large variety of pulse regimes [22,23]. Chromatic dispersion also plays a fundamental role for multiwavelength lasers, into which a four-wave-mixing process has been shown to assist in tuning the wavelength separation and enhancing the stability of multiwavelength emission [24–26]. The wide transparency of ChG glass to mid-IR wavelengths also makes ChG microwires a promising building block for mid-IR fiber lasers while using an appropriate gain medium [27].

In this Letter, we report the first mode-locked fiber laser based on a As_2S_3-PMMA ChG microwire. The microwire has a length of 10 cm and exhibits a waveguide nonlinearity that is 10^4 times that of SMF-28. The fiber laser is passively mode-locked with nonlinear polarization rotation (NPR) [28],

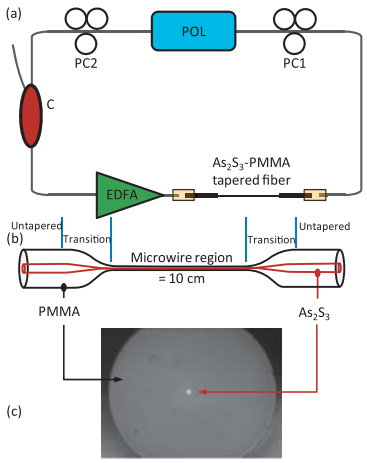

Fig. 1. (a) Experimental setup of the proposed EDF laser. POL, polarizer; C, coupler; PC, polarization controller. (b) Schematic of the tapered fiber. (c) Input facet of the hybrid fiber.

and generates noise-like pulses and soliton pulses with tunable central wavelengths. The laser also emits multiwavelength spectra with tunable central wavelength, switchable wavelength separation, and a variable number of laser wavelengths.

The experimental setup of the proposed erbium-doped fiber (EDF) laser is illustrated in Fig. 1(a). It consists of a commercial EDF amplifier, polarization controllers (PCs), a 99/1% coupler (C), a linear polarizer (POL), and a tapered ChG As_2S_3 fiber. The EDF amplifier has a built-in polarization-independent isolator that ensures unidirectional operation of the laser. The nonlinear medium enables the fiber laser to self-pulsate from NPR.

Figures 1(b) and 1(c), respectively, show a schematic and input facet of the hybrid fiber used in the experiment. The hybrid fiber is made of an As_2S_3 core surrounded by a PMMA cladding, and its central part is tapered down adiabatically into a 10 cm long microwire using a tapering process described in [20]. The core size in the untapered region is 14 μm and is reduced down to 1.7 μm in the microwire region. Each untapered and transition region of the fiber is $L_{\text{unt}} = 2$ cm and $L_{\text{trans}} = 3$ cm long, with a group velocity dispersion (GVD) of $\beta_{2,\text{unt}} = 457$ ps^2/km and $\langle\beta_{2,\text{trans}}\rangle = 369$ ps^2/km, respectively.

Both ends of the hybrid fiber are butt-coupled to an SMF-28, and the fibers are bonded permanently with UV epoxy. The measured total insertion loss is 6 dB including Fresnel reflection losses (2 × 0.45 dB), mode-mismatch at the hybrid fiber-SMF interfaces (2 × 0.65 dB), microwire surface roughness losses (2 dB) [29], and the remaining is attributed to misalignment at the SMF-As_2S_3 interfaces.

The GVD (β_2) and waveguide nonlinearity (γ) of the microwire are determined by solving the characteristic equation of an infinite cladding cylindrical waveguide to obtain the propagation constant β, the electric field distribution $\vec{E}$, and the magnetic field distribution $\vec{H}$ for the fundamental mode [30]. Figure 2 depicts the calculated GVD and waveguide nonlinearity of SMF-28 and As_2S_3-PMMA microwire with a 1.7 μm diameter. The microwire is of normal dispersion ($\beta_{2,\text{mic}} = 80$ ps^2/km) at a wavelength of 1550 nm and with a zero-dispersion wavelength at 1625 nm. The total length of the laser cavity is 26.5 m including 16.3 m of SMF-28 with anomalous dispersion ($\beta_{2,\text{SMF}} = -12.8$ ps^2/km), 10 m of EDF with normal dispersion ($\beta_{2,\text{EDF}} = 5$ ps^2/km), and 20 cm As_2S_3-PMMA tapered fiber with average-normal dispersion ($\langle\beta_2\rangle = 245$ ps^2/km). Thus, the proposed EDF laser operates with net anomalous dispersion due to SMF-28.

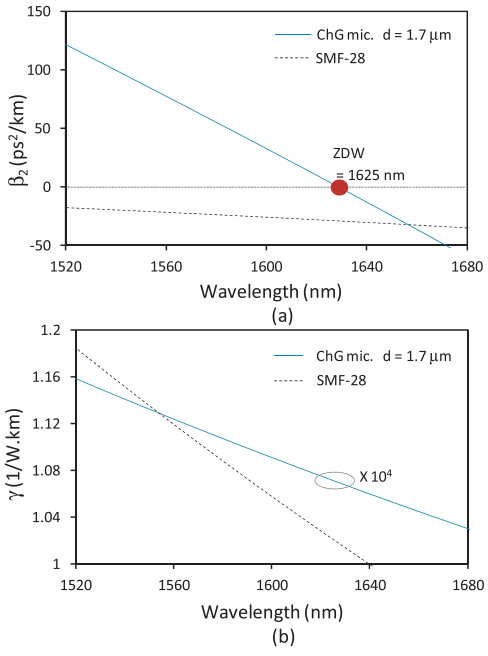

Fig. 2. (a) Dispersion and (b) waveguide-nonlinearity profiles of SMF-28 and As_2S_3-PMMA microwire with a diameter of 1.7 μm.

Figure 2(b) shows that the waveguide nonlinearity of an As_2S_3-PMMA microwire with a diameter of 1.7 μm is 10^4 times that of SMF-28. The waveguide nonlinearity of the microwire is 11.3 W^{-1} m^{-1} at a wavelength of 1550 nm. The high nonlinearity of the ChG microwire, with respect to SMF-28, allows mode-locking operation at low signal powers as well as reducing the fiber length required for sufficient nonlinearity in the cavity.

The microwire is fabricated with a modal birefringence from a residual stress applied by the PMMA cladding to the As_2S_3 core. This type of birefringence is controllable over some extent by adjusting the tapering temperature. Figure 3 shows the experimental measurement (black solid line) and theoretical calculation (red dashed line) for the wavelength dependence of light transmittance through crossed polarizers [31]. The interference peaks are separated by 2 nm, which corresponds to a birefringence $B_m = \lambda^2/\Delta\lambda L_{\text{mic}} = 1.12 \times 10^{-2}$, where L_{mic} is the length of the microwire.

Theoretical calculation of light transmittance is determined from [32]

$$T = \cos^2\theta_1 \cos^2\theta_2 + \sin^2\theta_1 \sin^2\theta_2 + \frac{1}{2}\sin 2\theta_1 \sin 2\theta_2 \times \cos(\Delta\Phi_L + \Delta\Phi_{\text{NL}}), \quad (1)$$

where Φ_L is the linear phase shift resulting from modal birefringence; Φ_{NL} is the nonlinear phase shift whose magnitude is the sum of the self-phase modulation and cross-phase modulation contributions; θ_1 is the angle between the axis of the polarizer (POL1) and the fast axis of microwire; and θ_2 is the angle between the axis of the polarizer (POL2) and the fast axis of microwire.

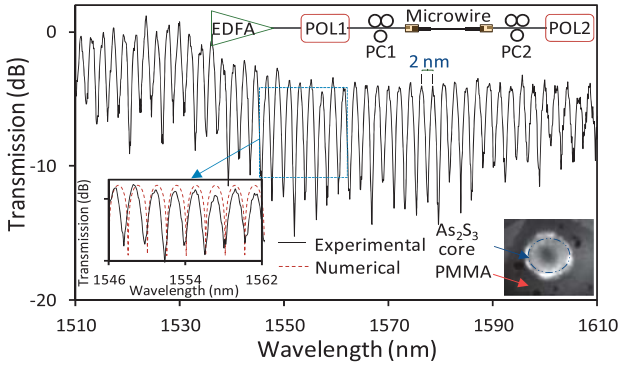

Fig. 3. Measured (black solid line) and calculated (red dotted line) wavelength dependence of light transmittance from a POL1-PC1-microwire-PC2-POL2 structure shown in the top of the figure. The insets in the bottom show an overlap of experimental and theoretical calculation of light transmittance (left inset) as well as an image of the hybrid fiber facet (right inset).

The operation principle of the ChG microwire-based multifunction NPR laser is described as follows. Linearly polarized light leaving the polarizer is made elliptical by PC2. The light then splits into two components with different intensities as it enters the birefringent microwire. Along the microwire, each component experiences a different nonlinear phase shift due to the Kerr effect. The total state-of-polarization of the light rotates in the microwire, and the angle of rotation is dependent on the magnitude of light intensity. Then, the light passes through PC1 and the polarizer (acts here as analyzer), which allows only polarization components parallel to its axis to pass through. Therefore, the combination of PC2-microwire-PC1-POL acts as an intensity-dependent element [33,34].

Soliton pulses are generated by a proper adjustment of the PCs such that high-intensity light propagates through the polarizer and low-intensity light is absorbed. In this regime, the PC-microwire-PC-POL functions as a saturable absorber. Figure 4(a) shows the spectra of a typical train of solitons under various powers. The threshold signal power at which solitons are formed in the cavity is ~11 mW. The peak power of solitons increases as the pump power increases. The soliton spectrum is centered at a wavelength of 1562 nm. The Kelly sidebands support the solitonic behavior of the laser output. These sidebands are a consequence of sudden changes in the losses, dispersion, and nonlinearity between As_2S_3-PMMA microwire and SMF-28, which prevent the soliton from adapting adiabatically [35]. The repetition rate of the laser is 7.8 MHz, which corresponds to a cavity length of 26.5 m.

A soliton with higher peak power can be achieved by balancing the path-averaged dispersion of the cavity. There are two methods to compensate the chirp accumulated in the cavity which can be concluded from the following equation:

$$2\beta_{\{2,\mathrm{unt}\}}L_{\mathrm{unt}} + 2\langle\beta_{\{2,\mathrm{trans}\}}\rangle L_{\mathrm{trans}} + \beta_{\{2,\mathrm{mic}\}}L_{\mathrm{mic}} = \beta_{\{2,\mathrm{SMF}\}}L_{\mathrm{SMF}} + \beta_{\{2,\mathrm{EDF}\}}L_{\mathrm{EDF}}. \quad (2)$$

The first method is to increase the length of the microwire to $L_{\mathrm{mic}} = 243$ cm. However, the propagation loss for such a length would be limited by the surface roughness of the microwire. A more practical method is to fabricate a 10 cm long microwire with a diameter of 0.56 μm, rather than 1.7 μm. Such microwire exhibits a normal GVD with $\beta_2 = 1195$ ps^2/km, which can compensate the anomalous dispersion of SMF-28.

The central wavelength of the generated soliton can be switched from $\lambda_{S1} = 1530$ nm to $\lambda_{S2} = 1562$ nm by adjusting the PCs. Figure 4(b) shows two soliton spectra measured at different θ_1 and θ_2 with a signal power of 56 mW.

At higher signal powers, the NPR laser generates noise-like pulses [36]. The threshold signal power for such pulses to be generated is 60 mW. Figure 5 shows the noise-like pulse spectra as a function of signal power. The large bandwidth observed is a consequence of the relatively high energy that noise-like pulses exhibit at the repetition rate of the cavity. One explanation for the generation of such pulses by NPR lasers is the combined effect of soliton collapse and positive cavity feedback [37].

Multiwavelength lasing occurs as well by properly adjusting the PCs so that higher intensity light experiences higher losses. In this regime, the PC-microwire-PC-POL functions as a Lyot birefringence filter [10,14,34]. The power threshold to achieve multiwavelength lasing is the lowest of all three regimes, i.e., 450 μW. This is due to the strong nonlinear birefringence induced by the As_2S_3-PMMA microwire. At this power, four lasing wavelengths are generated with a wavelength separation of 2 nm, a central wavelength of 1531 nm, and a power difference among lasing wavelengths of 4 dB. Figure 6(a) presents the multiwavelength emission at this signal power. The number of lasing wavelengths increases to 5 by increasing the signal power to 11 mW.

At a signal power of 11 mW, the central wavelength of a multiwavelength emission is tuned from 1531.3 to 1561.3 nm by adjusting the PCs, as shown in Fig. 6(a). The maximum power difference and signal-to-noise ratio among lasing wavelengths is 6 and 43 dB, respectively. The signal-to-noise ratio can be improved further by reducing the coupling losses between the SMF-28 and the As_2S_3-PMMA microwire. To examine the stability of the laser, the power of the central line of each spectra is measured over a time of 4 min, as shown in Fig. 6(b). The results reveal that multiwavelength emission at 1531.3 and 1560.9 nm wavelengths vary within a power range of 0.88 and 0.49 dB,

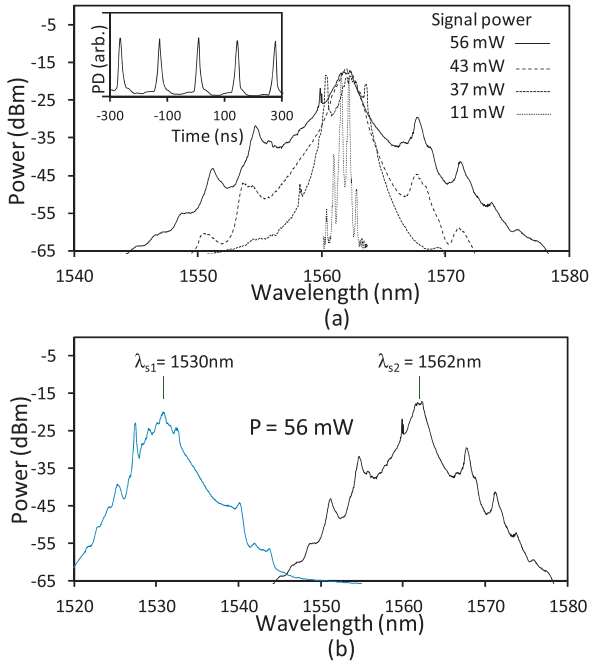

Fig. 4. Output spectra of fiber laser operating in soliton regime at (a) different signal powers, (b) different polarization state. The inset in (a) shows the trains of solitons in the time domain.

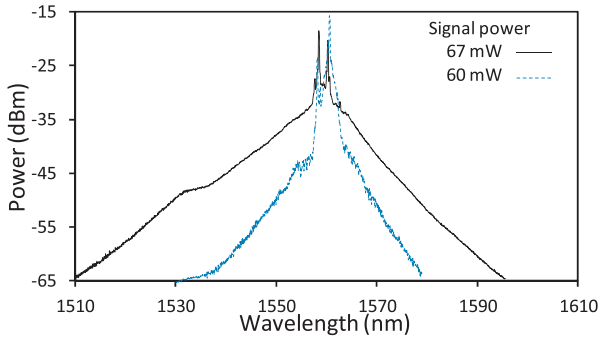

Fig. 5. Output spectra at different signal powers for noise-like pulse regime.

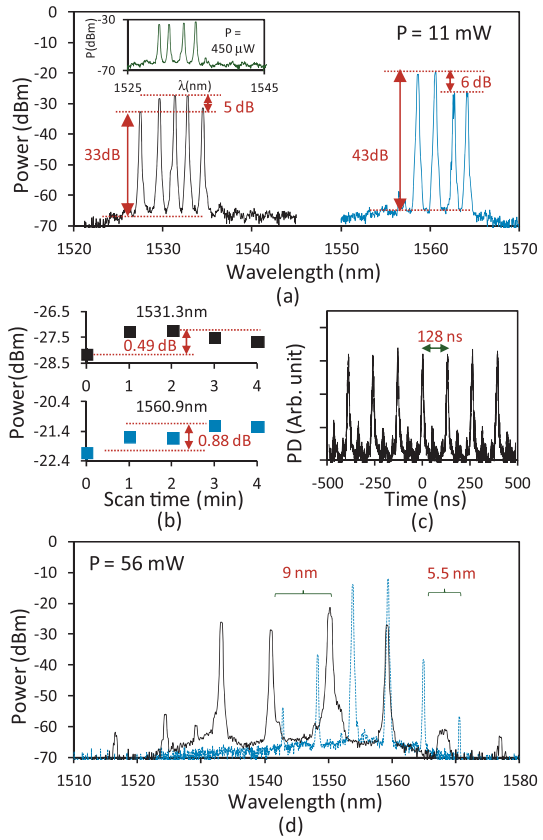

Fig. 6. (a) Multiwavelength emission measured with different polarization states at signal powers of 450 μW and 11 mW. (b) Stability of multiwavelength emission within a scanning time of 4 min. (c) Pulse trains of multiwavelength emission. (d) Multiwavelength emission measured with different polarization state at a pump power of 56 mW.

respectively. In the time domain, the oscilloscope trace exhibits a pulse train at the fundamental repetition rate of 7.8 MHz, as shown in Fig. 6(c).

The wavelength separation between spectral lines can also be switched by adjusting the PCs and increasing the signal power. Figure 6(d) shows multiwavelength emissions at a signal power of 56 mW with a wavelength separation changing from 5.5 to 9 nm by adjusting the PCs.

In conclusion, we have introduced the first NPR fiber laser using an As_2S_3-PMMA microwire as the nonlinear medium. The laser generates soliton pulses, with a tunable central wavelength from 1530 to 1562 nm at a threshold signal power of 11 mW, and noise-like pulses at a central wavelength of 1560 nm using a signal power of 60 mW. The laser also emits stable multiwavelength spectra at a threshold power of 450 μW with tunable central wavelength from 1531.3 to 1561.3 nm, switchable wavelength separation (2, 5.5, and 9 nm), and a variable number of laser wavelengths (4 and 5). The use of a chalcogenide (ChG) microwire reduces the nonlinear medium length of NPR lasers by 4 orders of magnitude with respect to silica fiber-based NPR lasers. The use of a ChG microwire results in the realization of laser operation at microwatt-level threshold powers.

Funding. Canada Foundation for Innovation (CFI); Fonds de recherche du Québec - Nature et Technologies (FQRNT) Equipe (173906).

REFERENCES

1. M. E. Fermann and I. Hartl, IEEE J. Sel. Top. Quantum Electron. **15**, 191 (2009).
2. D. Brida, G. Krauss, A. Sell, and A. Leitenstorfer, Laser Photon. Rev. **8**, 409 (2014).
3. Y. Han, T. Tran, S. Kim, and S. Lee, Opt. Lett. **30**, 1282 (2005).
4. M. Bello-Jiménez, C. Cuadrado-Laborde, D. Sáez-Rodríguez, A. Diez, J. Cruz, and M. Andrés, Opt. Lett. **35**, 3781 (2010).
5. E. Kuzin, B. Ibarra Escamilla, D. Garcia-Gomez, and J. Haus, Opt. Lett. **26**, 1559 (2001).
6. N. Seong and D. Kim, Opt. Lett. **27**, 1321 (2002).
7. X. Liu and Y. Cui, Sci. Rep. **3**, 2718 (2013).
8. M. Horowitz, Y. Barad, and Y. Silberberg, Opt. Lett. **22**, 799 (1997).
9. Z. Q. Luo, J. Z. Wang, M. Zhou, H. Y. Xu, Z. P. Cai, and C. C. Ye, Laser Phys. Lett. **9**, 229 (2012).
10. A. C. Song, W. Xu, Z. Luo, A. Luo, and W. Chen, Opt. Commun. **282**, 4408 (2009).
11. X. H. Feng, H. Y. Tan, C. Lu, P. K. Wai, and B. O. Guan, IEEE Photon. Technol. Lett. **21**, 1314 (2009).
12. A. Luo, Z. Luo, and W. Xu, Opt. Lett. **34**, 2135 (2009).
13. X. Liu, L. Zhan, J. Liu, and X. Shen, IEEE Photon. Technol. Lett. **25**, 1737 (2013).
14. Z. Zhang, K. Xu, J. Wu, X. Hong, and J. Lin, IEEE Photon. Technol. Lett. **20**, 979 (2008).
15. O. Pottiez, A. Martinez-Rios, D. Monzon-Hernandez, G. Salceda-Delgado, J. C. Hernandez-Garcia, B. Ibarra-Escamilla, and E. A. Kuzin, Laser Phys. **23**, 035103 (2013).
16. T. North and M. Rochette, Opt. Lett. **37**, 716 (2012).
17. R. Ahmad and M. Rochette, Appl. Phys. Lett. **101**, 101110 (2012).
18. D. Yeom, E. Mägi, M. Lamont, M. Roelens, L. Fu, and B. J. Eggleton, Opt. Lett. **33**, 660 (2008).
19. C. Baker and M. Rochette, Opt. Express **18**, 12391 (2010).
20. C. Baker and M. Rochette, IEEE Photon. J. **4**, 960 (2012).
21. T. A. Birks, W. J. Wadsworth, and P. St. J. Russell, Opt. Lett. **25**, 1415 (2000).
22. S. Kobtsev, S. Smirnov, S. Kukarin, and S. Turitsyn, Opt. Fiber Technol. **20**, 615 (2014).
23. Z. Shao, X. Qiao, Q. Rong, and D. Su, Opt. Commun. **345**, 105 (2015).
24. X. Liu, X. Zhou, and C. Lu, Opt. Lett. **30**, 2257 (2005).
25. Z. Zhang, L. Zhan, K. Xu, J. Wu, Y. Xia, and J. Lin, Opt. Lett. **33**, 324 (2008).
26. X. S. Liu, L. Zhan, X. Hu, H. G. Li, Q. S. Shen, and Y. X. Xia, Opt. Commun. **282**, 2913 (2009).
27. M. Bernier, V. Fortin, N. Caron, M. El-Amraoui, Y. Messaddeq, and R. Vallée, Opt. Lett. **38**, 127 (2013).
28. A. B. Han, S. Lou, H. Zou, W. Su, C. Liu, and J. Zhang, Laser Phys. **24**, 045103 (2014).
29. G. Zhai and L. Tong, Opt. Express **15**, 13805 (2007).
30. A. W. Snyder and J. D. Love, *Optical Waveguide Theory* (Chapman & Hall, 1983).
31. D. Derickson, *Fiber Optic Test and Measurement* (Prentice Hall, 1998).
32. L. Caiyun, W. Jian, W. Boyu, and G. Yizhi, IEEE Photon. Technol. **10**, 1250 (1998).
33. X. H. Feng, H. Y. Tam, and P. K. A. Wai, Opt. Express **14**, 8205 (2006).
34. A. M. Weiner, *Ultrafast Optics* (Wiley, 2009).
35. H. Haus, K. Tamura, L. Nelson, and E. Ippen, IEEE J. Quantum Electron. **31**, 591 (1995).
36. S. Kobtsev, S. Kukarin, S. Smirnov, S. Turitsyn, and A. Latkin, Opt. Express **17**, 20707 (2009).
37. Y. Jeong, L. Vazquez-Zuniga, S. Lee, and Y. Kwon, Opt. Fiber Technol. **20**, 575 (2014).